Materials International
Open-Access Journal (ISSN: 2668-5728)

Article
Volume 7, Issue 3, 2025, 21
https://doi.org/10.33263/Materials73.021

Influence of Carbon Nanotubes on Flow, Heat, and Mass Transfer of Hybrid Nanofluid Past a Stretched Sheet with Chemical Reaction

Prasanta Parida [1], **Hibah Islahi** [2], **Kharabela Swain** [3,*]

[1] Research Scholar, Institute of Applied Sciences, Mangalayatan University, Aligarh-202146, India; 20230218_prasanta@mangalayatan.edu.in;
[2] Institute of Applied Sciences, Mangalayatan University, Aligarh-202146, India; hibah.islahi@mangalayatan.edu.in;
[3] Department of Mathematics, GIFT Autonomous, Bhubaneswar-752054, India; kharabela1983@gmail.com;
* Correspondence: kharabela1983@gmail.com; kharabelaswain@gift.edu.in;

Received: 2.09.2024; Accepted: 15.08.2025; Published: 10.09.2025

Abstract: Hybrid nanofluid (HNF) has a wide range of heat transfer applications in industries like manufacturing, microelectronics, pharmaceutical, microfluidics, and many others due to their high effective thermal conductivity as compared to ordinary fluids and nanofluids (NF). An analysis is made of the steady flow of incompressible HNF past a stretching sheet, combined with first-order slip subjected to uniform suction or blowing. We have considered water H_2O as a base fluid and Single-Walled Carbon Nanotubes (SWCNT), Multi-Walled Carbon Nanotubes (MWCNT) as nanoparticles. The momentum equation includes the effect of the magnetic field, whereas the energy equation is influenced by viscous dissipation and Joule heating, and the concentration equation accounts for chemical reaction. The governing PDEs are converted into a system of ODEs using suitable similarity transformations. The numerical solution is obtained with the help of MATLAB software using the bvp4c solver. The results and discussion section highlight the key effects of the characterizing parameters in the present study. A few important findings are as follows. Suction/injection has a powerful effect on concentration as well as temperature distribution. Nusselt number (Nu_x) remains positive throughout the table, leading to heat energy flows from the plate to the fluid $(T_W > T_\infty)$; it indicates cooling of the bounding surface. This model works as a heat exchanger. Further, an increase in the slip parameter (λ_3) from 0.1 to 0.5 gives rise to an increase in heat flux of 2.71% and a decrease in $|C_f|$ 44.91% and Sh_x 2.2% at the bounding surface, respectively.

Keywords: chemical reaction; suction/injection; Joule heating; viscous dissipation; stretching sheet.

1. Introduction

Stretching/shrinking sheets are used in the present model to characterize the heat and momentum transport of the fluid flow. Given the manifold applications of carbon nanotubes as nanoparticles in various base fluids, many researchers [1-3] have contributed significantly to this field.

Hybrid nanofluid (HNF) has recently been considered by many researchers [4-7] to develop different models using water and ethylene glycol as base fluids, and metallic and metallic oxide nanoparticles with different volume fractions (i.e., concentrations). Usually, metal nanoparticles such as Cu, Ag etc., and metallic oxides (Fe_2O_3, Al_2O_3,CuO), materials of carbon (graphite, CNTs, SWCNTs, MWCNTs), metal carbide, and metal nitride are frequently used by the researchers [8-11]. Besides these factors, nanoparticle size, nanoparticle form, and nanoparticle solid volume fraction are crucial for optimizing the thermal conductivity of the HNF considered in the model.

Furthermore, suction/injection at the bounding surfaces is of great interest to many researchers, and most importantly, the model explicitly incorporates the Brownian motion and thermophoresis as the primary slip mechanisms affecting nanoparticle behavior. Brownian motion refers to the random motion of nanoparticles due to collisions with base fluid molecules, whereas thermophoresis describes the movement of nanoparticles from hotter to cooler regions. As regards external forces like the magnetic field, the electric field is negligible or of very low intensity. Moreover, most models use diluted nanofluid when the nanoparticle volume fraction is relatively low. The above models find applications in cooling electronic components such as microchips, nuclear reactor cooling, and heat exchangers. In the extended sense, the model can be used in biomedical and nuclear waste repositories. Devi and Devi [12] investigated the MHD flow of nanofluid past a porous elongating sheet using copper and alumina as nanoparticles. Gumber *et al*. [13] studied the micropolar HNF flow past a vertical plate. The effects of hybrid copper and silver nanoparticles flowing past a vertical plate are studied by Rawat *et al*. [14]. Upreti *et al*. [15] studied Ag-H_2O nanofluid flow over a porous vertical flat plate in the presence of Ohmic dissipation, heat source/sink, and suction/injection.

Magnetohydrodynamics (MHD) in nanofluids plays a pivotal role in boundary-layer flows, as the application of magnetic fields enables precise manipulation of fluid motion, thereby enhancing flow stability, heat transfer performance, and overall system efficiency. MHD has a wide range of applications in industry, including heat exchangers, MHD pumps, generators, geothermal energy extractors, flow meters, and space vehicle propulsion [16]. Swain *et al*. [17] studied the dissipative effects of a non-uniform heat source/sink on MHD flow of Williamson NF through porous medium under convective boundary conditions. Mahanthesh *et al*. [18] studied Darcy–Forchheimer flow of a Casson fluid in a circular tube subjected to the energy losses due to the viscous heating and Joule dissipation. Many authors [19-22] have studied the MHD flow of nanofluid and hybrid nanofluid using different flow geometries.

The MHD flow under the influence of thermal radiation has always been an interesting area for researchers. Thermal radiation affects the concentration of molecules and increases temperature by increasing energy and molecular motion. The inclusion of thermal radiation further improves the system's efficiency, and the addition of motile microorganisms enhances the nanoparticles' heat transfer performance. Ghadikolaei *et al*. [23] found that the radiation parameter diminishes the temperature contour when the fluid flows between two identical plates. Khan *et al*. [24] prepared an analytical model to analyze solar radiative Carreau nanofluid flow past a sheet with variable thickness. Hasona *et al*. [25] comprehensively developed a mathematical model to study the peristaltic motion of Carreau NFs. Zainal *et al*. [26] studied the thermal radiation effect on stagnation point flow of Maxwell hybrid nanofluid. Many researchers [27–29] have contributed significant studies in these areas.

The effects of chemical reactions on heat and mass transfer have wide-ranging applications across industries such as food processing, materials production, geothermal energy systems, and chemical process technology. Numerous studies have investigated the influence of chemical reactions on the flow, heat, and mass transfer over stretching surfaces. The presence of a chemical reaction can significantly alter the concentration field, thereby affecting both the mass transfer rate and the associated heat transfer characteristics. Mahabaleshwar *et al*. [30] studied the MHD HNF flow over a porous elongating sheet with quadratic velocity. Maranna *et al*. [31] examined the two-dimensional biviscous Bingham tetra-hybrid nanofluid flow past a permeable accelerated plate while accounting for suction/injection, slip conditions, and chemical reactions. Amudhini and Poulomi [32] investigated the Soret–Dufour effects on unsteady MHD flow of tetra-hybrid nanofluid past a non-Darcy porous stretching cylinder with chemical reactions and multiple slip boundary conditions. Arulmozhi et al. [33] and Veera Krishna and Vijaya Kumar [34] studied the MHD NF flow over a vertical plate and a stretching sheet, respectively, whereas Krishna *et al*. [35] investigated the Casson HNF over an exponentially vertical porous sheet. Ahammad and Krishna [36] discussed the combined effects of chemical reaction, Soret, and Dufour mechanisms on MHD free convection flow through a rotating perpendicular permeable channel. Lu *et al*. [37] illustrated unsteady hybrid nanofluid flow containing SWCNTs and MWCNTs as nanoparticles. Sunitha et al. [38] examined the chemically reactive Williamson NF over an exponentially elongating sheet.

Despite many interesting works reported in the literature, there is a deficiency in the handling of SWCNT and MWCNT nanoparticles with different base fluids, driven by industrial interest. To the best of our knowledge, earlier work has not considered Joule heating, which measures the resistance of the base fluid to the flow of electric current and generates thermal energy. Moreover, we have also considered viscous dissipation (the resistance offered by the fluid's viscosity) because some thermal energy is generated in the process. Specifically, we have considered the first-order velocity slip in this model. Usually, velocity slip occurs at the solid boundary for thin liquids. These aspects constitute the research gap that we have to address in the present work. Numerical solution is obtained for the transformed ODEs using the bvp4c code with the help of MATLAB software. The influences of physical parameters are described through tables and graphs.

2. Formulation of the Problem

Consider the steady, two-dimensional, laminar, and incompressible flow of HNF over a stretching sheet. The study comprises SWCNT and MWCNT nanoparticles in water (H2O) as the regular fluid; the sheet is placed along the *x*-axis, and the *y*-axis is normal to the sheet. A constant magnetic field strength B_0 is applied in the direction of the *y*-axis. The sheet is stretched with the velocity $u_w(x) = ax$ where $a > 0$ is constant, and the constant mass flux velocity is denoted by $v_0 = -\sqrt{a\nu_f}S$ where S is a constant. The surface and ambient temperatures and concentrations are, respectively T_w, T_∞ and C_w, C_∞. This model takes care of the cross flow, i.e., suction/injection at the bounding surface. The flow geometry of the present model is exhibited in Figure 1.

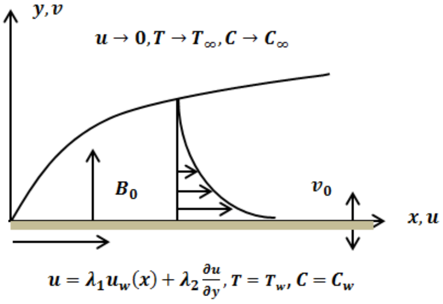

Figure 1. Flow geometry.

Using the above assumptions, the governing equations for steady flow of HNF following Devi and Devi [12] and Ahmad *et al*. [9] are:

$$\frac{\partial u}{\partial x}+\frac{\partial v}{\partial y}=0 \qquad (1)$$

$$u\frac{\partial u}{\partial x}+v\frac{\partial u}{\partial y}=\frac{\mu_{hnf}}{\rho_{hnf}}\frac{\partial^2 u}{\partial y^2}-\frac{\sigma_{hnf}}{\rho_{hnf}}B_0^2 u \qquad (2)$$

$$u\frac{\partial T}{\partial x}+v\frac{\partial T}{\partial y}=\frac{k_{hnf}}{(\rho C_p)_{hnf}}\left(1+\frac{16\sigma^*}{3k_{hnf}k^*}\right)\frac{\partial^2 T}{\partial y^2}+\frac{\sigma_{hnf}}{(\rho C_p)_{hnf}}B_0^2u^2+\frac{\mu_{hnf}}{(\rho C_p)_{hnf}}\left(\frac{\partial u}{\partial y}\right)^2 \qquad (3)$$

$$u\frac{\partial C}{\partial x}+v\frac{\partial C}{\partial y}=D_B\frac{\partial^2 C}{\partial y^2}-Kc(C-C_\infty) \qquad (4)$$

$$\left.\begin{array}{c} u=\lambda_1 u_w(x)+\lambda_2\frac{\partial u}{\partial y}, v=v_0, T=T_w, C=C_w\ at\ y=0 \\ u\to 0, T\to T_\infty, C\to C_\infty\ as\ y\to\infty \end{array}\right\} \qquad (5)$$

Consider the following dimensionless variables

$\psi=\sqrt{a\nu_f}xf(\eta),\eta=y\sqrt{a/\nu_f},\theta=\frac{T-T_\infty}{T_w-T_\infty},\Phi=\frac{C-C_\infty}{C_w-C_\infty}$ where ν_f is the kinematic viscosity, and the stream function ψ is defined as $u=\frac{\partial\psi}{\partial y}=axf'(\eta)$ and $v=-\frac{\partial\psi}{\partial x}=-(\sqrt{a\nu_f})f(\eta)$.

$$\frac{\mu_{hnf}/\mu_f}{\rho_{hnf}/\rho_f}f'''+ff''-f'^2-\frac{\sigma_{hnf}/\sigma_f}{\rho_{hnf}/\rho_f}Mf'=0 \qquad (6)$$

$$\frac{1}{Pr}\frac{1}{(\rho C_p)_{hnf}/(\rho C_p)_f}\left[\left(1+\frac{4}{3}R\right)\frac{k_{hnf}}{k_f}\theta''+f\theta'+\frac{\sigma_{hnf}}{\sigma_f}MEcf'^2+\frac{\mu_{hnf}}{\mu_f}Ecf''^2\right]=0 \qquad (7)$$

$$\Phi''+Sc(f\Phi'-\gamma\Phi)=0 \qquad (8)$$

$$\left.\begin{array}{c} f(0)=S, f'(0)=\lambda_1+\lambda_3 f''(0), \theta(0)=1\,, \Phi(0)=1, \\ f'^{(\infty)}\to 0, \theta(\infty)\to 0, \Phi(\infty)\to 0 \end{array}\right\} \qquad (9)$$

Here, $v_0=-\sqrt{a\nu_f}S$ where S is the constant mass flux parameter and $S>0, S=0\,, S<0$ are respectively for suction, impermeable, and injection cases. Further, $\lambda_1>0, \lambda_1=0, and\ \lambda_1<0$ represents the stretching, rigid, and shrinking cases, respectively.

The friction coefficient (C_f), Nusselt number (Nu_x) and Sherwood number (Sh_x) are defined as:

$$C_f=\frac{\mu_{hnf}}{u_w^2\rho_f}\left(\frac{\partial u}{\partial y}\right)_{y=0}\Rightarrow Re_x^{1/2}C_f=\frac{\mu_{hnf}}{\mu_f}f''(0),$$

$$Nu_x=-\frac{x}{k_f(T_w-T_\infty)}\left\{k_{hnf}\left(\frac{\partial T}{\partial y}\right)_{y=0}+(q_r)_{y=0}\right\}\Rightarrow Re_x^{-1/2}Nu_x=-\left(\frac{k_{hnf}}{k_f}+\frac{4}{3}R\right)\theta'(0)$$

$$Sh_x=-\frac{x}{(C_w-C_\infty)}\left(\frac{\partial C}{\partial y}\right)_{y=0}\Rightarrow Re_x^{-1/2}Sh_x=-\Phi'(0)$$

Here, shear stress $\tau_w=\mu_{hnf}\left(\frac{\partial u}{\partial y}\right)_{y=0}$, heat flux $q_w=-k_{hnf}\left(\frac{\partial T}{\partial y}\right)_{y=0}$, mass flux $q_m=-D_B\left(\frac{\partial C}{\partial y}\right)_{y=0}$ and $Re_x=u_wx/\nu_f$ is the local Reynolds number.

Moreover, $\phi_1=\phi_2=0$ characterizes the regular fluid. Tables 1 and 2 represent the thermophysical properties of NF and HNF.

Table 1. Thermophysical properties of NF and HNF (Waini *et al*. [8]).

Properties	**Nanofluid**	**Hybrid nanofluid**
Density	$\rho_{nf}=(1-\phi_1)\rho_f+\phi_1\rho_{n1}$	$\rho_{hnf}=(1-\phi_2)[(1-\phi_1)\rho_f+\phi_1\rho_{n1}]+\phi_2\rho_{n2}$
Dynamic viscosity	$\mu_{nf}=\frac{\mu_f}{(1-\phi_1)^{2.5}}$	$\mu_{hnf}=\frac{\mu_f}{(1-\phi_1)^{2.5}(1-\phi_2)^{2.5}}$

Properties	Nanofluid	Hybrid nanofluid
Thermal conductivity	$\frac{k_{nf}}{k_f} = \frac{k_{n1} + 2k_f - 2\phi_1(k_f - k_{n1})}{k_{n1} + 2k_f + \phi_1(k_f - k_{n1})}$	$\frac{k_{hnf}}{k_{nf}} = \frac{k_{n2} + 2k_{nf} - 2\phi_2(k_{nf} - k_{n2})}{k_{n2} + 2k_{nf} + \phi_2(k_{nf} - k_{n2})}$
Heat capacity	$(\rho C_p)_{nf} = (1-\phi_1)(\rho C_p)_f + \phi_1(\rho C_p)_{n1}$	$(\rho C_p)_{hnf} = (1-\phi_2)\begin{bmatrix}(1-\phi_1)(\rho C_p)_f \\ +\phi_1(\rho C_p)_{n1}\end{bmatrix} + \phi_2(\rho C_p)_{n2}$
Electrical conductivity	$\frac{\sigma_{nf}}{\sigma_f} = 1 + \frac{3\left(\frac{\sigma_{n1}}{\sigma_f} - 1\right)\phi_1}{\frac{\sigma_{n1}}{\sigma_f} + 2 - \left(\frac{\sigma_{n1}}{\sigma_f} - 1\right)\phi_1}$	$\frac{\sigma_{hnf}}{\sigma_{nf}} = 1 + \frac{3\left(\frac{\sigma_{n2}}{\sigma_{nf}} - 1\right)\phi_2}{\frac{\sigma_{n2}}{\sigma_{nf}} + 2 - \left(\frac{\sigma_{n2}}{\sigma_{nf}} - 1\right)\phi_2}$

Table 2. Thermo-physical properties of water and nanoparticles (Sreenivasulu *et al.* [22]).

Properties	$\rho(kg/m^3)$	$C_p(J/kgK)$	$k(W/mK)$	$\sigma(\Omega^{-1}m^{-1})$
water	997	4179	0.613	0.05
$SWCNT$	2600	425	6600	4.8×10^7
$MWCNT$	1600	796	3000	3.3×10^6

Table 3. Comparison of $-\theta'(0)$ for different values of Pr when $M = Ec = Sc = \gamma = 0$ and $\lambda_1 = 1$.

Pr	**Devi and Devi [12]**	**Khan and Pop [1]**	**Ahmad *et al.* [9]**	**Present study**
2	0.91135	0.9113	0.91045	0.911353
7	1.89540	1.8954	1.89083	1.895409
20	3.35390	3.3539	3.35271	3.353940
70	----	6.4621	6.47814	6.462262

3. Results and Discussion

The numerical solution is obtained for the system of non-linear ODEs (7) – (9), applying MATLAB software with the bvp4c code for the step size 10^{-2}. The convergence, stability, and accuracy have been tested for the solution. The error tolerance is set to be 10^{-5}. Further, to validate the numerical code, we have compared our results with Devi and Devi [12], Khan and Pop [1], and Ahmad *et al.* [9], and presented them in Table 3. The range of physical parameters considered in the present study is as follows: $0 \leq M, Ec, R \leq 1, 0.1 \leq \lambda_1, \lambda_3 \leq 1, 0 \leq \phi_1, \phi_2 \leq 0.1, -2 \leq S \leq 3, 2 \leq Sc \leq 5$ and $-1 \leq \gamma \leq 1$. To bring out the effects of the characteristics parameters on the flow and heat transfer of hybrid nanofluid, such as magnetic field (measure of Lorentz force) and Eckert number (measure of the dissipation effect), on the nano and hybrid nanofluid, differentiating between metallic and metallic oxide nanoparticles. The following are the three important thermal energy sources either generated or applied in the fluid flow, such as viscous dissipation, which leads to the heating of the fluid constantly, consequently, temperature increases; Joule heating is due to the resistance of the fluid to flow of electric current, and heat source is the additional thermal energy released per mole of the fuel used.

Figure 2 exhibits the velocity profiles depicting the effects of the magnetic field on base fluid, $SWCNT$-water, $MWCNT$-water, and hybrid nanofluid. It is observed that the base fluid offers maximum resistance to flow, so that the base fluid attains the minimum velocity as the magnetic field strength increases. The hybrid nanofluid attains the highest velocity in comparison with the base fluid as well as the nanofluid. All the profiles attain the ambient state asymptotically.

Figure 3 shows the effect of the velocity slip parameter (λ_3) for fixed values of the stretching parameter (λ_1). It is observed that an increase in the velocity slip parameter results in a decrease in the velocity, whereas the opposite effect is observed in the case of the stretching parameter (λ_1). It is interesting to note that for low values of the slip parameter, a sharp fall in velocity is marked. On the other hand, when the slip parameter increases, the fall slows down the velocity and attains the ambient state in a short span of space variable (η). So it is useful to design requirements when needed.

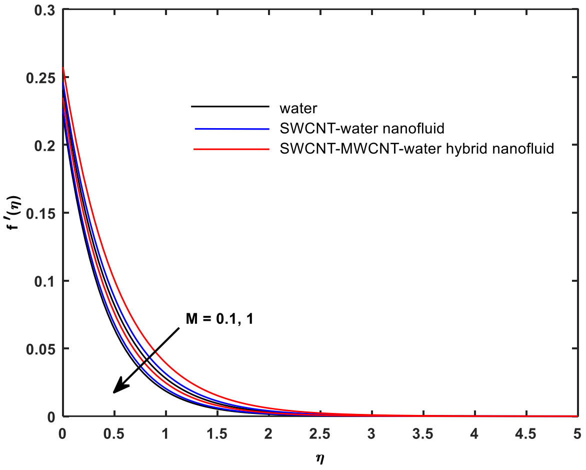

Figure 2. Velocity profiles versus M.

Figure 4 indicates the variation of velocity versus suction/injection. The outcome is quite trivial as the velocity increases for injection $(S < 0)$ and decreases for suction $(S > 0)$. It is also seen that, for suction, the curvature of the velocity profile is significant, whereas for injection it is much less, approaching a straight line. Therefore, it leads to a conclusion that for high suction, the shear-free flow is achieved instantly within a small span of the space variable (η) which is always desirable.

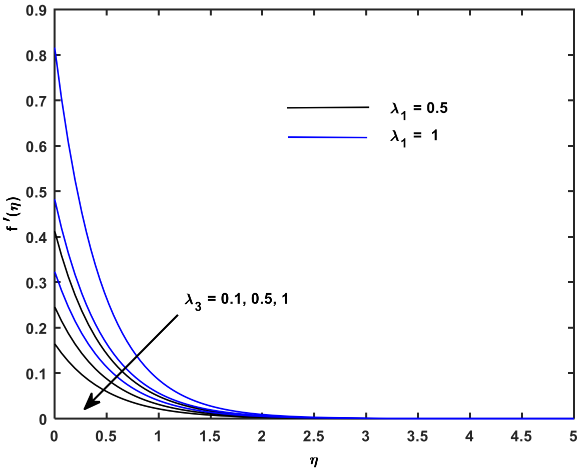

Figure 3. Velocity profiles versus λ_1 and λ_3.

Figure 5 presents the variation of temperature with respect to volume fraction of $SWCNT\ (\phi_1)$ for a fixed value of volume fraction of $MWCNT\ (\phi_2)$. A noteworthy observation is that the combined effect of ϕ_1 and ϕ_2 escalates the thermal energy considerably; consequently, the temperature of the flow domain increases, which is what is expected from the present model. To summarize, both NF and HNF energize the thermal system.

Figure 6 presents a very interesting phenomenon of symetricity in temperature distribution about a line joining two points $(0,1)$ and $(2,0)$ in the coordinate system η and θ. In other words, suction and injection are two important phenomena in boundary-layer control systems. It is observed that suction reduces the temperature, indicating a depletion of thermal energy, whereas injection has the opposite effect. The symmetry of temperature profiles claims special attention in the present flow model.

Figure 7 shows the variation of temperature with respect to Eckert number and stretching/squizzing parameter. As the Eckert number is a measure of the quantum of dissipative energy, the increase in it contributes to higher temperature. It means the energy generated by friction is transferred to the fluid mass, increasing its thermal energy. This is true for both stretching and squizzing at the boundary wall.

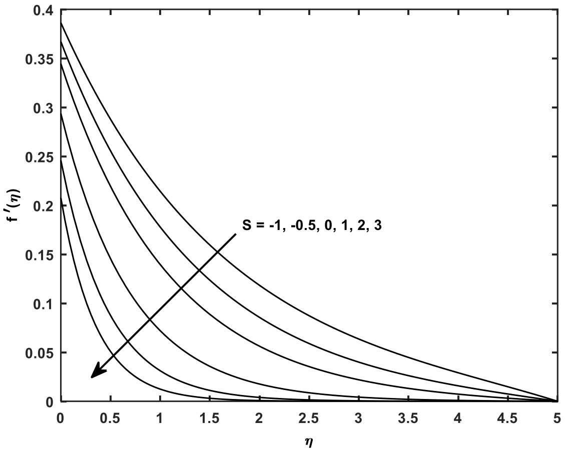

Figure 4. Velocity profiles versus S.

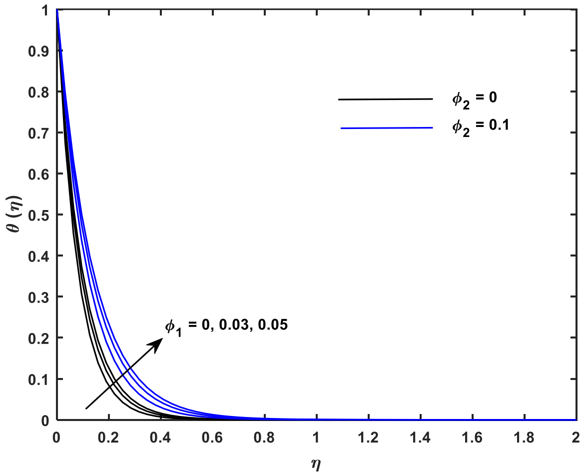

Figure 5. Temperature profiles versus ϕ_1 and ϕ_2.

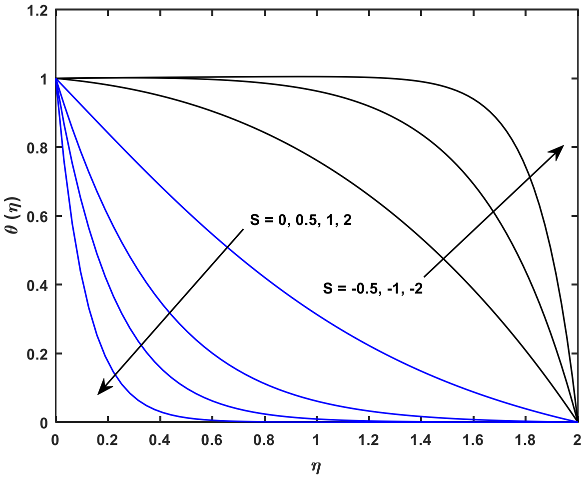

Figure 6. Temperature profiles versus S.

Figure 8 also shows the temperature distribution for different values of thermal radiation parameter (R). It is observed that the thermal radiation significantly influences the temperature field. With an increase in the thermal radiation parameter, the temperature distribution within the boundary layer is enhanced. Larger values of the radiation parameter correspond to greater absorption of thermal energy by the fluid, which increases the fluid temperature and, consequently, thickens the thermal boundary layer. This behavior highlights the role of radiation as a heating mechanism in the present flow model.

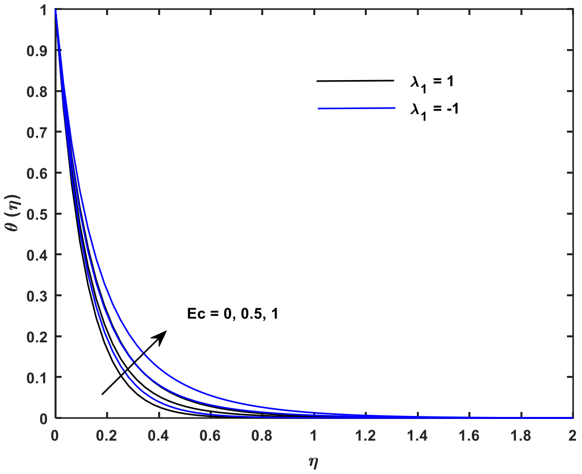

Figure 7. Temperature profiles versus Ec and λ_1.

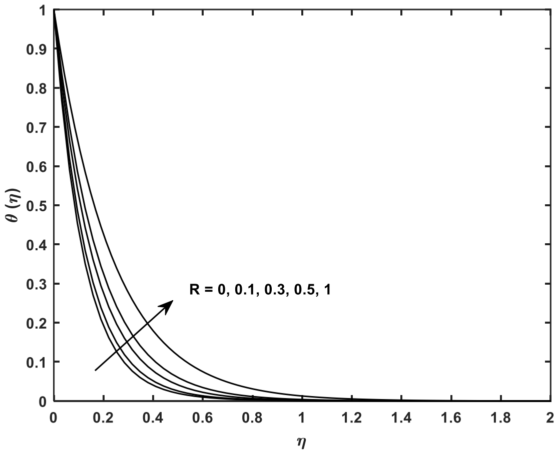

Figure 8. Temperature profiles versus R.

Figure 9 presents the variation of concentration for different values of Schmidt number (Sc). The values prescribed for $Sc = 3, 4, 5$ relate to diffusion of species through a thin liquid medium. Now, comparing with Figure 6, the variation of temperature with respect to suction/injection, it is evident that the phenomena of suction/injection retain their symmetry when the concentration varies as well. Therefore, it is affirmed that suction/injection has an overpowering effect on concentration as well as temperature distribution.

Figure 10 depicts the concentration profile for various values of the chemical reaction parameter for both destructive/exothermic ($\gamma > 0$)and a constructive/endothermic reaction ($\gamma < 0$). The molar concentration of HNF decreases with the increase in destructive reaction, and the reverse effect is observed for constructive reaction. The concentration profile exhibits the characteristic temperature dependence, i.e., asymptotic approach to the ambient state.

Table 4 presents the numerical values of three important criteria related to the bounding surface of the flow domain, i.e., interface fluxes affecting substantially the characteristics of the flow domain (momentum, thermal, and solutal transport) for constant volume fraction of $SWCNT$ and $MWCNT$ and $Pr = 6.2, Sc = 2.0$.

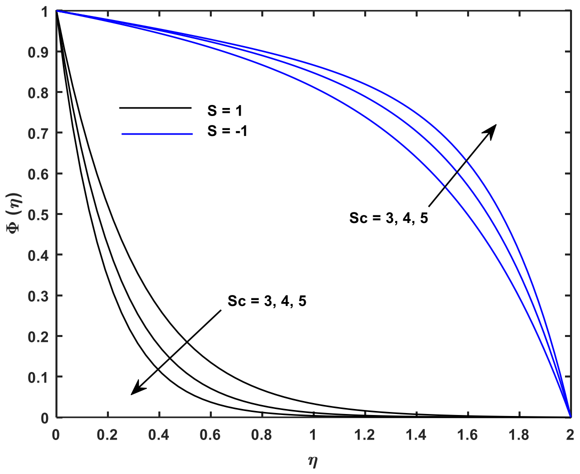

Figure 9. Concentration profiles versus Sc and S.

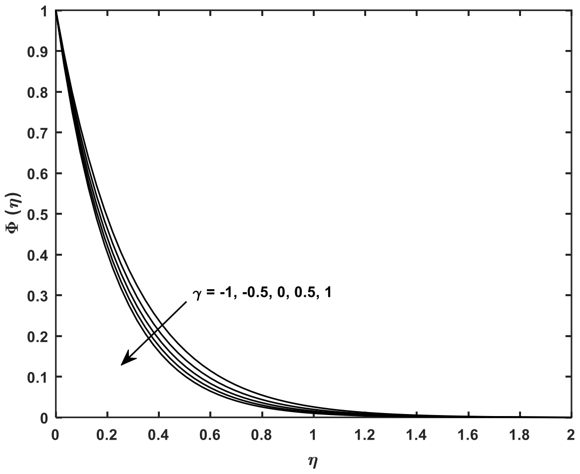

Figure 10. Concentration profiles versus γ.

At the outset, it is observed that the skin friction coefficient remains negative throughout, irrespective of variations in other parameters. This shows that no flow reversal occurs in the flow model since $f''(0) < 0$. Another point is to note that the Nusselt number (Nu_x) remains positive throughout the table, leading to heat energy flows from the plate to the fluid $(T_w > T_\infty)$; it indicates cooling of the bounding surface. This model works as a heat exchanger. A similar conclusion can be drawn with respect to the Sherwood number (Sh_x) as it remains positive throughout, also. This inference remains valid for solutal concentration at the bounding surface for the fluid with a low Schmidt number $(Sc = 2.0)$. Though the present model deals with the flow of NF and HNF, this correlates to the mixture of air with ethyl benzene where $Sc = 2.0$. It is seen that an increase in the magnetic parameter slightly decreases Nu_x and Sh_x but $|C_f|$ increases. Further, it is seen that an increase in λ_1 increases the modulus of C_f and (Sh_x) but (Nu_x) decreases. The effect of λ_3 is opposite to that of λ_1. Moreover, an increase in the suction parameter $(S > 0)$ gives rise to a decrease in the Nu_x and Sh_x.

Table 4. Computational values of C_f, Nu_x and Sh_x when $\phi_1 = \phi_2 = 0.05, Pr = 6.2,$ and $Sc = 2$.

M	λ_1	λ_3	R	Ec	γ	S	C_f	Nu_x	Sh_x
0	0.1	0.1	0.1	0.1	0.1	2	-0.197707	11.938565	4.078405
0.5							-0.218124	11.935395	4.076950
1							-0.235241	11.932804	4.075769
	0.5						-1.217503	11.939035	4.171478
	1						-2.528432	11.600343	4.281179
		0.5					-1.392893	11.915106	4.187194

M	λ_1	λ_3	R	Ec	γ	S	C_f	Nu_x	Sh_x
		1					-0.899773	11.963939	4.142037
			0.3				-0.899772	12.539010	4.142037
			0.5				-0.899772	12.967450	4.142037
				0.3			-0.899772	12.322632	4.142037
				0.5			-0.899772	12.106255	4.142037
					0.5		-0.899772	12.106255	4.320074
					1		-0.899772	12.106255	4.525371
					0		-0.899772	12.106255	4.095232
					-0.5		-0.899772	11.193430	3.844206
					-1		-0.899772	11.193430	3.555839
					0.5	1	-0.811724	5.989388	2.556214
						0	-0.709632	0.807912	1.174241
						-1	-0.606852	-0.428062	0.480021
						-2	-0.516437	-0.299893	0.251842

4. Quantitative analysis

Quantitative analysis of tabular data runs as: Increase in slip parameter. (λ_3) from 0.1 to 0.5 gives rise to an increase in heat flux of 2.71% and a decrease in $|C_f|$ 44.91% and Sh_x 2.2% at the bounding surface, respectively. Thus, it is concluded that the slip parameter produces a significant change in surface criteria to affect the flow, heat, and solutal transfer in hybrid nanofluid.

Figure 3 shows the velocity variation: When $\lambda_1 = 1, \lambda_3 = 0.1$ then $f'(0) = 0.816128$; $\lambda_1 = 0.5, \lambda_3 = 0.1$ then $f'(0) = 0.412432$. From this data, it is evident that the velocity at the boundary decreases nearly 50% when the stretching rate decreases 50%. For $\lambda_1 = 1, \lambda_3 = 0.5$; $f'(0) = 0.482322$, the velocity at the boundary decreases 40.9% when the slip parameter (λ_3) increases from 0.1 to 0.5.

5. Conclusion

From the present study, it is found that the hybrid nanofluid exhibits the highest velocity compared to the base fluid and the nanofluid, and that all velocity profiles attain the ambient state asymptotically. For low values of the slip parameter, a sharp fall in velocity is marked, whereas an increase in the slip parameter decreases the velocity. So it is desirable in flow control applications. Suction reduces the temperature, indicating depletion of thermal energy, whereas injection produces a reverse effect. The symmetry of temperature and concentration profiles claims special attention in the present flow model. Therefore, it is affirmed that suction/injection has an overpowering effect on concentration as well as temperature distribution. Nusselt number (Nu_x) remains positive throughout the table, leading to heat energy flows from the plate to the fluid $(T_w > T_\infty)$; it indicates cooling of the bounding surface. This model works as a heat exchanger. Increase in slip parameter (λ_3) from 0.1 to 0.5 gives rise to an increase in heat flux of 2.71% and a decrease in $|C_f|$ 44.91% and Sh_x 2.2% at the bounding surface, respectively.

The present model can be extended to non-Newtonian fluids such as Casson fluid, Powell–Eyring fluid, and Phan–Thien–Tanner fluid. It can further be generalized to account for flow through a porous medium, which has wide applications in industry and scientific research. Additionally, the model may be extended to incorporate thermal slip and solutal slip conditions at the boundary.

Author Contributions

Conceptualization, P.P., H.I., and K.S.; methodology, P.P., H.I., and K.S.; software, K.S.; writing—original draft preparation, P.P., H.I., and K.S.; writing—review and editing, K.S.; supervision, H.I. and K.S. All authors have read and agreed to the published version of the manuscript.

Institutional Review Board Statement

Not applicable.

Informed Consent Statement

Not applicable.

Data Availability Statement

Data supporting the findings of this study are available upon reasonable request from the corresponding author.

Funding

This research received no external funding.

Acknowledgement

The authors thank Prof. (Dr.) G. C. Dash, Research Professor, Department of Mathematics, SOA (Deemed to be University), for his sincere effort to revise the manuscript. Also, the authors wish to express their very sincere thanks to the reviewers for their valuable comments and suggestions.

Conflicts of Interest

The authors declare no conflict of interest.

Abbreviations

The following abbreviations are used in this manuscript:

Abbreviation	Definition
x, y	Cartesian Coordinate System (m)
u, v	Velocity Components Along x, y Directions Respectively (m/s)
B_0	Magnetic Field Strength
T	Temperature
T_w	Temperature at the Sheet
T_∞	Ambient Temperature
k_{hnf}	Thermal Conductivity of Hybrid Nanofluid (m^2/s)
k_f	Thermal Conductivity of Base Fluid (m^2/s)
$Pr\left(=\frac{(\mu C_p)_f}{k_f}\right)$	Prandtl number
k_{nf}	Thermal Conductivity of Nanofluid (m^2/s)
$R\left(=\frac{4\sigma^* T_\infty^3}{3kk^*}\right)$	Radiation Parameter

D_B	Brownian Motion Coefficient (m^2/s)
S	Suction/Injection Parameter
v_0	Suction Velocity
$Ec\left(=\dfrac{u_w^2}{(C_p)_f(T_w-T_\infty)}\right)$	Eckert Number
$M\left(=\dfrac{\sigma_f B_0^2}{a\rho_f}\right)$	Magnetic Parameter
C_f	Local Skin Friction Coefficient
$Sc\left(=\dfrac{\nu_f}{D_B}\right)$	Schmidt Number
Kc^*	Rate of Chemical Reaction
$Kc\left(=\dfrac{Kc^*}{a}\right)$	Chemical Reaction Parameter
f	Dimensionless Velocity
Nu_x	Local Nusselt Number
Sh_x	Local Sherwood Number
Re_x	Local Reynolds Number
λ_1	Stretching Parameter
λ_2	Slip Constant
$\lambda_3\left(=\lambda_2\sqrt{\dfrac{a}{\nu_f}}\right)$	Velocity Slip Parameter
ψ	Stream Function
θ	Dimensionless Temperature
Φ	Dimensionless Nanoparticle Volume Fraction
ν_{hnf}	Kinetic Velocity of Hybrid Nanofluid (m^2/s)
ρ_f	Density of Base Fluid (kg/m^3)
ρ_{nf}	Density of Nanofluid (kg/m^3)
ρ_{nf}	Density of Hybrid Nanofluid (kg/m^3)
σ_{hnf}	Electrical Conductivity of Hybrid Nanofluid $(\Omega^{-1}m^{-1})$
σ_{nf}	Electrical Conductivity of Nanofluid $(\Omega^{-1}m^{-1})$
μ_{hnf}	Viscosity of Hybrid Nanofluid (kg/m s)
μ_{nf}	Viscosity of Nanofluid (kg/m s)
$(\rho C_p)_{hnf}$	Heat Capacitance of Hybrid Nanofluid (J/kg K)
$(\rho C_p)_{nf}$	Heat Capacitance of Hybrid Nanofluid (J/kg K)

References

1. Khan, W.A.; Pop, I. Boundary-layer flow of a nanofluid past a stretching sheet. *Int. J. Heat Mass Transf.* **2010**, *53*, 2477-2483, https://doi.org/10.1016/j.ijheatmasstransfer.2010.01.032.
2. Swain, K.; Animasaun, I.L.; Ibrahim, S.M. Influence of exponential space-based heat source and Joule heating on nanofluid flow over an elongating/shrinking sheet with an inclined magnetic field. *Int. J. Ambient Energy* **2022**, *43*, 4045-4057, https://doi.org/10.1080/01430750.2021.1873854.
3. Panigrahi, L.; Panda, J.; Swain, K.; Dash, G.C. Heat and mass transfer of MHD Casson nanofluid flow through a porous medium past a stretching sheet with Newtonian heating and chemical reaction. *Karbala Int. J. Mod. Sci.* **2020**, *6*, 11, https://doi.org/10.33640/2405-609X.1740.
4. Swain, K.; Mishra, S. Flow and heat transfer analysis of water-based copper nanofluid over a nonlinearly stretching sheet: a numerical approach. *Int. J. Ambient Energy* **2022**, *43*, 5810–5824, https://doi.org/10.1080/01430750.2021.1995490.

5. Al-Kouz, W.; Swain, K.; Mahanthesh, B.; Jamshed, W. Significance of exponential space-based heat source and inclined magnetic field on heat transfer of hybrid nanoliquid with homogeneous–heterogeneous chemical reactions. *Heat Transfer* **2021**, *50*, 4086-4102, https://doi.org/10.1002/htj.22065.
6. Swain, K.; Mebarek-Oudina, F.; Abo-Dahab, S.M. Influence of MWCNT/Fe_3O_4 hybrid nanoparticles on an exponentially porous shrinking sheet with chemical reaction and slip boundary conditions. *J. Therm. Anal. Calorim.* **2022**, *147*, 1561-1570, https://doi.org/10.1007/s10973-020-10432-4.
7. Ramzan, M.; Dawar, A.; Saeed, A.; Kumam, P.; Watthayu, W.; Kumam, W. Heat transfer analysis of the mixed convective flow of magnetohydrodynamic hybrid nanofluid past a stretching sheet with velocity and thermal slip conditions. *PLOS ONE* **2021**, *16*, e0260854, https://doi.org/10.1371/journal.pone.0260854.
8. Waini, I.; Ishak, A.; Pop, I. Hybrid Nanofluid Flow over a Permeable Non-Isothermal Shrinking Surface. *Mathematics* **2021**, *9*, 538, https://doi.org/10.3390/math9050538.
9. Ahmad, S.; Ali, K.; Rizwan, M.; Ashraf, M. Heat and mass transfer attributes of copper–aluminum oxide hybrid nanoparticles flow through a porous medium. *Case Stud. Therm. Eng.* **2021**, *25*, 100932, https://doi.org/10.1016/j.csite.2021.100932.
10. Eid, M.R.; Mahny, K.L.; Dar, A.; Muhammad, T. Numerical study for Carreau nanofluid flow over a convectively heated nonlinear stretching surface with chemically reactive species. *Phys. A: Stat. Mech. Appl.* **2020**, *540*, 123063, https://doi.org/10.1016/j.physa.2019.123063.
11. Triveni, K.; Mahanthesh, B. Heat transport of hybrid nanomaterial in an annulus with quadratic Boussinesq approximation. *Appl. Math. Mech.-Engl. Ed.* **2021**, *42*, 885-900, https://doi.org/10.1007/s10483-021-2739-6.
12. Devi, S.P.A.; Devi, S.S.U. Numerical Investigation of Hydromagnetic Hybrid Cu – Al_2O_3/Water Nanofluid Flow over a Permeable Stretching Sheet with Suction. *Int. J. Nonlinear Sci. Numer. Simul.* **2016**, *17*, 249-257, https://doi.org/10.1515/ijnsns-2016-0037.
13. Gumber, P.; Yaseen, M.; Rawat, S.K.; Kumar, M. Heat transfer in micropolar hybrid nanofluid flow past a vertical plate in the presence of thermal radiation and suction/injection effects. *P. Differ. Equ. Appl. Math.* **2022**, *5*, 100240, https://doi.org/10.1016/j.padiff.2021.100240.
14. Rawat, S.K.; Mishra, A.; Kumar, M. Numerical study of thermal radiation and suction effects on copper and silver water nanofluids past a vertical Riga plate. *Multidiscip. Model. Mater. Struct.* **2019**, *15*, 714-736, https://doi.org/10.1108/MMMS-07-2018-0129.
15. Upreti, H.; Pandey, A.K.; Kumar, M. MHD flow of Ag-water nanofluid over a flat porous plate with viscous-Ohmic dissipation, suction/injection and heat generation/absorption. *Alex. Eng. J.* **2018**, *57*, 1839-1847, https://doi.org/10.1016/j.aej.2017.03.018.
16. Babazadeh, H.; Shah, Z.; Ullah, I.; Kumam, P.; Shafee, A. Analysis of hybrid nanofluid behavior within a porous cavity including Lorentz forces and radiation impacts. *J. Therm. Anal. Calorim.* **2021**, *143*, 1129-1137, https://doi.org/10.1007/s10973-020-09416-1.
17. Swain, K.; Parida, S.K.; Dash, G.C. Effects of Non-Uniform Heat Source/Sink and Viscous Dissipation on MHD Boundary Layer Flow of Williamson Nanofluid through Porous Medium. *Defect and Diffusion Forum* **2018**, *389*, 110-127, https://doi.org/10.4028/www.scientific.net/DDF.389.110.
18. Mahanthesh, B.; Al-Kouz, W.; Swain, K.; Rout, P.K. Computational modeling of heat transfer in magneto-non-Newtonian material in a circular tube with viscous and Joule heating. *Heat Transf.* **2021**, *50*, 6703-6718, https://doi.org/10.1002/htj.22199.
19. Ojha, K.L.; Swain, K.; Dash, P. Viscoelastic hydromagnetic oscillatory flow in a channel in the presence of sinusoidal pressure gradient and linear motion of the plate. *Heat Transf.* **2022**, *51*, 1138-1149, https://doi.org/10.1002/htj.22345.
20. Swain, K.; Mahanthesh, B. Thermal Enhancement of Radiating Magneto-Nanoliquid with Nanoparticles Aggregation and Joule Heating: A Three-Dimensional Flow. *Arab. J. Sci. Eng.* **2021**, *46*, 5865–5873, https://doi.org/10.1007/s13369-020-04979-5.
21. Yaseen, M.; Kumar, M.; Rawat, S.K. Assisting and opposing flow of a MHD hybrid nanofluid flow past a permeable moving surface with heat source/sink and thermal radiation. *Partial Differ. Equ. Appl. Math.* **2021**, *4*, 100168, https://doi.org/10.1016/j.padiff.2021.100168.
22. Sreenivasulu, P.; Gunakala, S.R.; Poornima, T.; Reddy, N.B.; Job, V.M. Aligned magnetic field and Navier slip effects on free convective radiative flow of nanofluids with imbedded carbon nanotubes: a Lie group analysis. *SN Appl. Sci.* **2020**, *2*, 1283, https://doi.org/10.1007/s42452-020-3105-5.

23. Ghadikolaei, S.S.; Hosseinzadeh, K.; Ganji, D.D. Analysis of unsteady MHD Eyring-Powell squeezing flow in stretching channel with considering thermal radiation and Joule heating effect using AGM. *Case Stud. Therm. Eng.* **2017**, *10*, 579-594, https://doi.org/10.1016/j.csite.2017.11.004.
24. Khan, M.; Malik, M.Y.; Salahuddin, T. Heat generation and solar radiation effects on Carreau nanofluid over a stretching sheet with variable thickness: Using coefficients improved by Cash and Carp. *Results Phys.* **2017**, *7*, 2512–2519, https://doi.org/10.1016/j.rinp.2017.06.048.
25. Hasona, W.M.; Almalki, N.H.; ElShekhipy, A.A.; Ibrahim, M.G. Thermal radiation and variable electrical conductivity effects on MHD peristaltic motion of Carreau nanofluids: Radiotherapy and thermotherapy of oncology treatment. *Heat Transfer—Asian Res.* **2019**, *48*, 938–956, https://doi.org/10.1002/htj.21415.
26. Zainal, N.A.; Nazar, R.; Naganthran, K.; Pop, I. The Impact of Thermal Radiation on Maxwell Hybrid Nanofluids in the Stagnation Region. *Nanomaterials* **2022**, *12*, 1109, https://doi.org/10.3390/nano12071109.
27. Waini, I.; Ishak, A.; Pop, I. Hybrid nanofluid flow and heat transfer over a nonlinear permeable stretching/shrinking surface. *Int. J. Numer. Meth. Heat Fluid Flow* **2019**, *29*, 3110-3127, https://doi.org/10.1108/HFF-01-2019-0057.
28. Khashi'ie, N.S.; Arifin, N.M.; Nazar, R.; Hafidzuddin, E.H.; Wahi, N.; Pop, I. Magnetohydrodynamics (MHD) axisymmetric flow and heat transfer of a hybrid nanofluid past a radially permeable stretching/shrinking sheet with Joule heating. *Chin. J. Phys.* **2020**, *64*, 251-263, https://doi.org/10.1016/j.cjph.2019.11.008.
29. Reddy, T.S.; Roja, P.; Ibrahim, S.M.; Lorenzini, G. Thermal Radiation and Viscous Dissipation Effects on (MHD) Bioconvection Stream of Maxwell Nanoliquid over a Permeable Vertical Plate Due to Gyrotactic Microorganisms. *Math. Model. Eng. Probl.* **2022**, *9*, 325–335, https://doi.org/10.18280/mmep.090205.
30. Mahabaleshwar, U.S.; Anusha, T.; Hatami, M. The MHD Newtonian hybrid nanofluid flow and mass transfer analysis due to super-linear stretching sheet embedded in porous medium. *Sci. Rep.* **2021**, *11*, 22518, https://doi.org/10.1038/s41598-021-01902-2.
31. Maranna, T.; Mahabaleshwar, U.S.; Huang, H.N.; Joo, S.W. An Analytical Inspection on Effect of Chemical Reaction and Radiation on MHD Biviscous Bingham Tetra Nanofluid Flow With Accelerated Plate. *J. Nanotechnol.* **2025**, *2025*, 1382579, https://doi.org/10.1155/jnt/1382579.
32. Amudhini, M.; De, P. Comparative study of hybrid, tri-hybrid and tetra-hybrid nanoparticles in MHD unsteady flow with chemical reaction, activation energy, Soret-Dufour effect and sensitivity analysis over Non-Darcy porous stretching cylinder. *Heliyon* **2024**, *10*, e35731, https://doi.org/10.1016/j.heliyon.2024.e35731.
33. Arulmozhi, S.; Sukkiramathi, K.; Santra, S.S.; Edwan, R.; Fernandez-Gamiz, U.; Noeiaghdam, S. Heat and mass transfer analysis of radiative and chemical reactive effects on MHD nanofluid over an infinite moving vertical plate. *Results Eng.* **2022**, *14*, 100394, https://doi.org/10.1016/j.rineng.2022.100394.
34. Krishna, M.V.; Kumar, A.G.V. Chemical reaction, slip effects and non-linear thermal radiation on unsteady MHD Jeffreys nanofluid flow over a stretching sheet. *Case Stud. Therm. Eng.* **2024**, *55*, 104129, https://doi.org/10.1016/j.csite.2024.104129.
35. Krishna, M.V.; Ahammad, N.A.; Chamkha, A.J. Radiative MHD flow of Casson hybrid nanofluid over an infinite exponentially accelerated vertical porous surface. *Case Stud. Therm. Eng.* **2021**, *27*, 101229, https://doi.org/10.1016/j.csite.2021.101229.
36. Ahammad, N.A.; Krishna, M.V. Numerical investigation of chemical reaction, Soret and Dufour impacts on MHD free convective gyrating flow through a vertical porous channel. *Case Stud. Therm. Eng.* **2021**, *28*, 101571, https://doi.org/10.1016/j.csite.2021.101571.
37. Lu, D.; Li, Z.; Ramzan, M.; Shafee, A.; Chung, J.D. Unsteady squeezing carbon nanotubes based nano-liquid flow with Cattaneo–Christov heat flux and homogeneous–heterogeneous reactions. *Appl. Nanosci.* **2019**, *9*, 169-178, https://doi.org/10.1007/s13204-018-0899-1.
38. Kumar, P.V.; Sunitha, C.; Lorenzini, G.; Ibrahim, S.M. A study of thermally radiant Williamson nanofluid over an exponentially elongating sheet with chemical reaction via homotopy analysis method. *CFD Lett.* **2022**, *14*, 68-86, https://doi.org/10.37934/cfdl.14.5.6886.

Publisher's Note & Disclaimer